Application of on-line FTIR methodology to study the mechanisms of heterogeneous advanced oxidation processes

Helen Barndõk, Noemi Merayo, Laura Blanco, Daphne Hermosilla [*], Ángeles Blanco

Department of Chemical Engineering, Universidad Complutense de Madrid, Avda. Complutense, s/n, 28040 Madrid, Spain

ARTICLE INFO

ABSTRACT

On-line FTIR-methodology was used to study the routes of 1,4-dioxane degradation in heterogeneous photocatalysis with titanium dioxide (TiO_2) and heterogeneous photo-Fenton with zero valent iron (Fe^0). To determine the multiple decomposition mechanisms of this environmental pollutant, heterogeneous Fe^0-catalyst was compared with a homogenous iron catalyst and different photocatalytic systems with UV radiation and solar light were studied. In addition, the influence of H_2O_2 addition profile was assessed to optimize of the reagent dose and reaction time. Complete removal of 1,4-dioxane and 85% mineralization of TOC were achieved by UV photo-Fenton with Fe^0, while solar light could work as cost-effective alternative, achieving 65% removal of 1,4-dioxane. Although constant addition of H_2O_2 was crucial for the rapid oxidation of organic matter, significant degradation was reached by only half of the stoichiometric amount of H_2O_2. Meanwhile, apparently similar treatment efficiencies were observed in both UV-assisted and solar photocatalysis (almost 60% of 1,4-dioxane removal). The degradation routes for 1,4-dioxane in both advanced oxidation processes were established and presented based on extensive chromatography analysis, whereas FTIR monitoring served as a powerful tool for on-line reaction monitoring. Ethylene glycol diformate was detected as the major primary intermediate in TiO_2-photocatalysis, whereas ethylene glycol was found as the main initial by-product in Fe^0-based photo-Fenton. An alternative route of 1,4-dioxane degradation through methoxyacetic and acetic acids was observed, being more pronounced in photo-Fenton processes and accentuated further in the presence of Fe^0.

1. Introduction

1,4-Dioxane is a common organic solvent, generated also as a by-product in many industrial processes [1]. Although this cyclic ether is classified as a B2 carcinogen due to its negative health effects [2–4], its removal by conventional processes is difficult due to its biorefractory and persistent nature [1,5–7]. Advanced oxidation processes (AOPs) are reported to effectively degrade 1,4-dioxane [8–11] through the formation of more biodegradable compounds, thus, reducing the overall cost of the process [12].

One of the most common AOPs, TiO_2-photocatalysis, is based on the combination of UV light and a semiconductor catalyst, offering several advantages like minimal production of residues and mild operation conditions suitable for environmental applications [13,14]. In contrast, another typical AOP, Fenton oxidation, is based

on the electron transfer between hydrogen peroxide (H_2O_2) and ferrous ion (Fe^{2+}). This process appears to be one of the most rapid and aggressive treatments suitable for heavily loaded industrial effluents [15,16]. However, during the last decade, combining both UV light and Fenton reaction in a so-called photo-Fenton process has become popular as an advantageous method due to the photo-recovery of catalytic Fe^{2+} and the photo-decarboxylation of the refractory ferric carboxylate complexes [17–23].

TiO_2-photocatalysis can achieve complete mineralization of 1,4-dioxane from diluted synthetic solutions [24,25]; however, elevated concentrations of this compound and other organic matter would require elevated concentrations of photocatalyst [26,27], causing a turbidity that inhibits the penetration of light and, thus, the activation of TiO_2. On the other hand, Fenton and photo-Fenton processes are limited by their optimal pH range (usually set at pH 3) [28,29] and iron sludge by-product that requires disposal [30]. Nevertheless, the use of zero valent iron (Fe^0) microspheres instead of Fe^{2+} salts can solve the drawbacks of photo-Fenton when working in heterogeneous conditions at neutral pH [31]. Moreover, moderate carbonaceous alkalinity was found beneficial to maintain the heterogeneous conditions without causing any

* Corresponding author.
E-mail addresses: hbarndok@quim.ucm.es (H. Barndõk), nmerayo@quim.ucm.es (N. Merayo), lblanco@quim.ucm.es (L. Blanco), dhermosilla@quim.ucm.es, dahermosilla@yahoo.es (D. Hermosilla), ablanco@quim.ucm.es (Á. Blanco).

significant negative effect on the process efficiency. Under neutral and slightly basic pH conditions the produced Fe^{2+} remains anchored on the surface of Fe^0 microspheres without Fe^{2+} leaching, thereby avoiding the subsequent generation of iron sludge [31].

Considering these heterogeneous AOPs, very few reports exist on the decomposition mechanisms of 1,4-dioxane during TiO_2-photocatalysis [32], and there is no literature on the identification of degradation routes and reaction intermediates formed along the treatment of 1,4-dioxane by heterogeneous photo-Fenton process using Fe^0, although some by-products have been identified [33,34]. Stefan and Bolton [35] proposed a degradation mechanism for 1,4-dioxane in UV/H_2O_2 oxidation, and Kim et al. [36] suggested a reaction pathway for homogeneous photo-Fenton reaction, both by exhaustive series of chromatographic methods.

As an alternative to the expensive and time-consuming chromatographic analysis, on-line fourier transform infrared (FTIR) spectroscopy has been successfully applied for the in situ control of the intermediate chemical species during the oxidation of 1,4-dioxane by classical Fenton [10] and ozonation [8] processes. Since the heterogeneous photocatalytic and photo-Fenton processes involve multiple possible transformations of catalyst and reactive radical species, different degradation routes could be expected, depending on the treatment. Moreover, on-line information of the whole reaction during the experiment would not only provide a straightforward understanding of the reaction mechanism, but also an accurate optimization of the reagent doses and reaction time, thus reducing the treatment cost.

Therefore, the main objective of this research was to establish the degradation routes for 1,4-dioxane treated by both heterogeneous photocatalysis with TiO_2 and heterogeneous photo-Fenton with Fe^0 and to study the mechanism of these processes under different radiation sources, using the on-line FTIR-methodology supported by extensive chromatography analysis. Furthermore, the FTIR tool was also applied for the optimization of the H_2O_2 required for the photo-Fenton process using Fe^0.

2. Materials and methods

2.1. Materials and analytical methods

All used reagents were of analytical grade and supplied by PANREAC S.A. (Barcelona, Spain) or Sigma–Aldrich (Highland, USA). Synthetic wastewater was prepared with $7050\,mg\,L^{-1}$ of 1,4-dioxane in deionized water. AEROXIDE® $P25-TiO_2$ (BET surface area = $50\,m^2\,g^{-1}$; pore volume = $0.25\,m^3\,g^{-1}$, and mean particle size of ca. 21 nm) was supplied by Evonik (Essen, Germany). Fe^0 microspheres (>98.3% Fe; <1% C; <1% N; <0.7% O) with 1 μm of particle size and $800\,m^2\,kg^{-1}$ of surface area were obtained from BASF (ZVI Microspheres 800, Ludwigshafen, Germany).

All the analyses were made according to the standard methods for the examination of water and wastewaters [37]. Chemical oxygen demand (COD) was measured by the colorimetric method at 600 nm using an Aquamate-spectrophotometer (Thermo Scientific AQA 091801, Waltham, USA). Total organic carbon (TOC) was measured by the combustion-infrared method using a TOC/TN analyser multi N/C® 3100 (Analytik Jena AG, Jena, Germany) with catalytic oxidation on cerium oxide at 850 °C. H_2O_2 concentration was analyzed by the titanium sulphate spectrophotometric method [38].

The FTIR analytical spectrometer ReacIR iC10 (Mettler-Toledo, Columbia, USA) was used to monitor chemical species as they react over a period of time as described by Merayo et al. [39]. In order to confirm the FTIR results, 1,4-dioxane and its degradation products, ethylene glycol diformate (EGDF) and ethylene glycol monoformate (EGMF), were identified and quantified by an Agilent 6890N gas chromatograph (GC, Palo Alto, CA) equipped with

a quadrupole mass spectrometer (MS) Agilent 5975B. To extract these two volatile compounds from the water samples, an internal standard ($5\,mg\,L^{-1}$ of octanol) and 1.4 g of ammonium sulphate were added to 10 mL of sample, and the solution was extracted threefold with dichloromethane (40:10:10 mL). The organic fraction was dried on anhydrous sodium sulphate and concentrated to 1 mL under nitrogen flux in a Kuderna–Danish apparatus (Sigma, St. Louis, MO) and subsequently analyzed by GC–MS as follows. Samples (3 μL) were injected in split mode (30:1) and volatiles were separated using a fused silica capillary column (HP-INNOWAX) ($30 × 0.25$ mm i.d. and 0.25-μm film thickness), supplied by Agilent (Madrid, Spain). The pressure of the GC-grade He carrier gas was 7.7 psi with a linear velocity of $1.0\,mL\,min^{-1}$; the initial oven temperature was 45 °C, which was first increased at $3\,°C\,min^{-1}$ up to 100 °C, held for 1 min, and then heated at $15\,°C\,min^{-1}$ up to 270 °C, and held at this temperature for an additional 5 min. The injection temperature was 230 °C. Detection was carried out by electron ionization (EI) mode (70 eV), interphase detection temperature was 290 °C (MS source at 230 °C and MS quad at 150 °C) and scanning mass was ranged between 35 and 400 amu. Quantitative determinations were carried out by the internal standard method, using peak areas obtained from selected ion (m/z) monitoring (88, 1,4-dioxane; 60, EGDF/EGMF; 45, octanol) and calibrations made with pure reference compounds analyzed under the same conditions.

1,4-Dioxane was also quantified together with ethylene glycol as its possible degradation product, using gas–liquid chromatography (GLC) on a 7980A instrument (Agilent Technologies Inc., Palo Alto, CA) equipped with a flame ionization detector. The temperatures of the injector and detector were 310 °C and 280 °C, respectively. Samples (2 μL) were injected using the pulsed-split mode (split ratio 5:1) and analyzed in a TRB-FFAP (Teknokroma, Sant Cugat del Vallès, Spain) fused silica column (30 m × 0.25 mm internal diameter × 0.25 μm film thickness) with He (43 psi) as carrier gas and the following temperature program: 80 °C to 240 °C after 9 min initial hold and at $15\,°C\,min^{-1}$ ramp rate. Peaks were identified according to the relative retention times of commercial standards. Quantification was performed according to peak area, corrected with the response factors calculated for each compound using 1-butanol (250 ppm) as internal standard, and the software GC-ChemStation Rev.B.04.02 (96) from Agilent.

Oxalic, acetic, formic, glycolic, and methoxyacetic acids were identified and quantified by ion chromatography (IC) using a 940 Professional IC Vario instrument (Metrohm, Herisau, Switzerland) equipped with a conductivity detector. An isocratic gradient of Na_2CO_3 (3.6 mM) was used as eluent, keeping an eluent flow at $0.7\,mL\,min^{-1}$. The injection loop was 50 mL. Analysis was done in an ionic resin column Metrosep A Supp 7 with a guard column Metrosep A Supp 4/5 Guard.

2.2. Experimental procedures

2.2.1. TiO_2 photocatalytic processes

Experiments were performed with $P25-TiO_2$ suspension of $10\,g\,L^{-1}$ [26,27] stirred on a magnetic mixing device. The initial pH of the 1,4-dioxane solution (≈5.7) was not modified. For the analyses, samples were withdrawn from the reactor and centrifuged for 15 min at $335 × g$, and then the supernatant was filtrated through 0.45 μm (PTFE syringe filter, Merck, Spain) to measure COD and TOC and analyze the possible reaction intermediates.

2.2.2. Fenton and photo-Fenton processes

Heterogeneous experiments with Fe^0 were performed in the presence of $1000\,mg\,L^{-1}$ $NaHCO_3$ buffer (pH_0 8.5), whereas the acidic conditions for homogeneous process with Fe^{2+} were obtained by adjusting the initial pH to 2.8 with 1 M H_2SO_4. In all the studied cases, pH was monitored along the process. After the

initial pH adjustment, iron was added to the 1,4-dioxane solution either in the form of Fe^0 microspheres at the optimum molar ratio $[H_2O_2]/[Fe^0] = 60$ found in preliminary experiments [31] or in the form of $FeSO_4$ at the optimum ratio of 5 found for the conventional Fenton process [10]. Batches of H_2O_2 (35% w/v) were then added in sequence until the total amount based on the stoichiometric ratio of $[H_2O_2]_0/[COD]_0 = 2.125$ was reached. After every sample withdrawal, an initial measurement of the H_2O_2 in the samples was made. Immediately afterward, the samples were adjusted to pH 9.0 by adding 40% NaOH, and then filtered through 0.45 μm to analyze the possible reaction intermediates and measure COD, TOC and remaining H_2O_2 concentrations. H_2O_2 concentration values were used to correct COD values according to Hermosilla et al. [28].

2.2.3. UV lamp and solar simulator

Experiments of UV/TiO_2 photocatalysis and UV photo-Fenton were performed at 25 °C, using a high-pressure mercury immersion lamp of 450 W from ACE-glass (Model 7825-30, Vineland, USA) placed in a quartz glass cooling jacket and located in a vertical manner in the centre of the glass reactor. Total volume of 1000 mL was treated, whereas the irradiated liquid surface per sample was $240 cm^2 L^{-1}$. The total photon flux of 1.1×10^{20} photon s^{-1} was calculated to flow inside the photochemical reactor as described by Liang et al. [40]. Light intensity measured on the irradiated liquid surface was $788 W m^{-2}$ at the mid-height of the UV-lamp (1.5 cm from the light source). Light intensity was recorded using UV–vis Radiometer RM-21 (UV-Elektronik, Ettlingen, Germany).

Solar TiO_2 photocatalysis and solar photo-Fenton trials were carried out in a Solar Simulator supplied by Newport (Irvine, USA), equipped with a Xe lamp (300 W) with a correction filter (ASTM E490-73a) to obtain the solar spectrum under ideal conditions. Total volume of 100 mL was treated, whereas the irradiated liquid surface per sample was $980 cm^2 L^{-1}$. The total photon flux was 6.8×10^{19} photon s^{-1}. The recorded light intensity was $444 W m^{-2}$ at 8 cm from the light source, which was the distance between the sample surface and the lamp.

To normalize the data in order to compare the results obtained with different liquid volumes and reactor configurations used in UV and solar enhanced processes, the light intensity recorded on the irradiated liquid surface in $W m^{-2}$ ($J s^{-1} m^{-2}$) was converted to $kJ L^{-1}$, taking into account the dimensions of the photoreactors.

3. Results and discussion

3.1. Heterogeneous photocatalysis with TiO_2

The photocatalytic degradation of 1,4-dioxane with TiO_2 powder was successfully monitored by FTIR probe. The comparison of the data from posterior chromatographic analysis (Fig. 1A) and on-line FTIR measurement (Fig. 1B) shows that the disappearance of a target molecule can be accurately observed in real time by tracking its characteristic peaks. According to the results of photocatalytic degradation of 1,4-dioxane on TiO_2, apparently similar treatment efficiencies were observed in both UV-assisted and solar photocatalysis (Fig. 1). About 45% of 1,4-dioxane was degraded when applying around $360 kJ L^{-1}$ of either solar or UV radiation, whereas almost 60% removal could be obtained in further irradiation in solar simulator ($470 kJ L^{-1}$). With both radiation sources, almost a linear degradation of 1,4-dioxane was observed ($\approx 7.5 mg kJ^{-1}$), according to both the chromatographic sample analysis and the on-line FTIR spectrometry, monitoring the peak at $1120 cm^{-1}$ characteristic to 1,4-dioxane spectra. This indicates that in both cases further removal of 1,4-dioxane is possible under longer radiation times.

Although the UV lamp with much greater potential than the solar simulator should lead to greater TiO_2 activation and, thus,
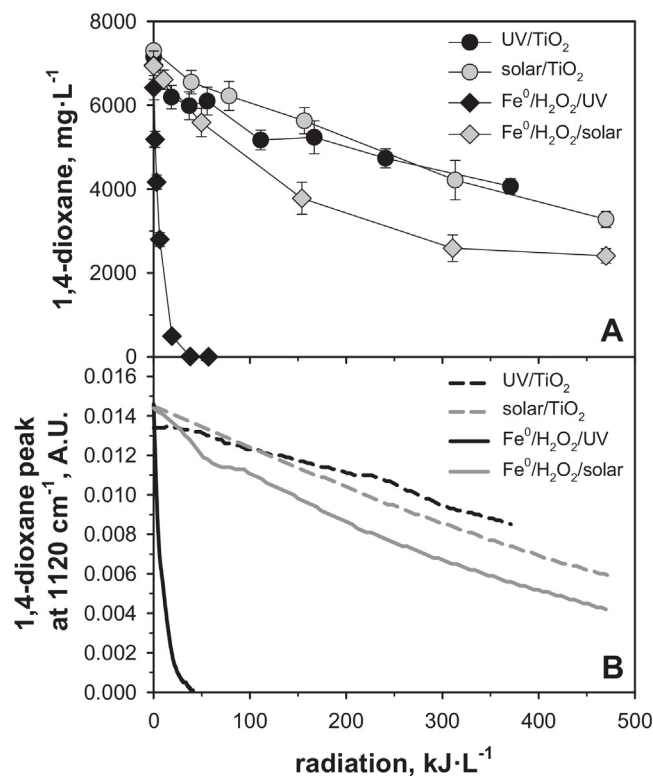

Fig. 1. Light assisted degradation of 1,4-dioxane during heterogeneous catalytic processes: (A) chromatographic analysis; (B) decrease of 1,4-dioxane peak in relative absorbance units (A.U.) monitored by FTIR spectrometry. $C_{0;dioxane} = 7050 mg L^{-1}$; pH_0 5.7 in TiO_2-based processes; pH_0 8.5 in Fe^0-based processes.

faster degradation kinetics, in this particular case, the configuration of the solar simulator above the surface of a rather thin water layer was more beneficial than the UV lamp immersed in a much larger water bulk (the intensity of light in a depth of 1 cm inside the turbid catalyst suspension was only 5% of the radiation on the liquid surface).

Regardless of the radiation source, both UV/TiO_2 and solar/TiO_2 processes led to very similar decomposition of 1,4-dioxane. Metabolites of 1,4-dioxane were observed in greater detail in the UV-catalyzed process (Fig. 2), in which EGDF and formic acid were identified as major reaction intermediates, generated alongside since the beginning of the reaction. Their evolution along the degradation process is well observed by chromatography after certain time-intervals (Fig. 2A); however, the on-line monitoring of the major characteristic peaks of FTIR spectra allows even clearer appreciation of the real trends of EGDF appearance and decay accompanied by the accumulation of formic acid (Fig. 2B). To a lesser extent, some acetic acid was produced along the process, while methoxyacetic and glycolic acids were detected as a mixture at concentrations below $5.6 \pm 0.2 mg L^{-1}$. Such low concentrations could not be detected with precision in the FTIR spectra. In addition, traces of EGMF ($\leq 0.03 \pm 0.01 mg L^{-1}$) were observed by GC–MS (data not shown).

3.2. Heterogeneous photo-Fenton processes with Fe^0

The heterogenous catalytic removal of 1,4-dioxane on Fe^0 microspheres was also successfully monitored with catalytic by the in situ FTIR measurement. As shown in Fig. 1, UV photo-Fenton process resulted in the greatest removal of 1,4-dioxane: less than $60 kJ L^{-1}$ of UV radiation was required to reach a complete removal of the compound along with 85% of TOC removals, whereas nearly
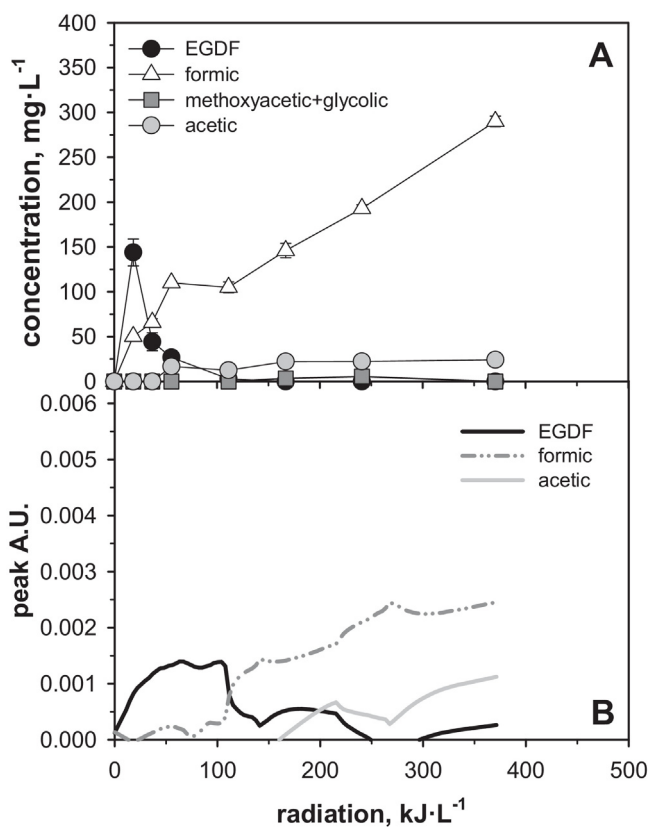
Fig. 2. Degradation products of 1,4-dioxane oxidation during UV/TiO$_2$ treatment: (A) chromatographic analysis; (B) FTIR monitoring of the major peaks in relative absorbance units (A.U.). $C_{0;dioxane}$ = 7050 mg L^{-1}; pH$_0$ 5.7.

Fig. 3. FTIR monitoring of the primary reaction intermediates (ethylene glycol or EGDF) during the oxidation of 1,4-dioxane by Fe^0-based UV photo-Fenton and UV/TiO$_2$ processes, respectively (peak height in relative absorbance units (A.U.)). $C_{0;dioxane}$ = 7050 mg L^{-1}; pH$_0$ 5.7 in UV/TiO$_2$; pH$_0$ 8.5 in Fe^0/H$_2$O$_2$/UV.

3.2.1. Fenton vs. photo-Fenton

Since Fe^0 can be activated already in the presence of H$_2$O$_2$ without light enhancement, an additional experiment of heterogeneous Fenton was carried out for comparison purposes. Radiation significantly contributed to the activation of the Fe^0 microspheres and, thus, to the treatment efficiency, as shown in Fig. 5. Without radiation, up to 25% of COD (and 45% of 1,4-dioxane) were removed by the heterogeneous Fenton oxidation with Fe^0 microspheres, which could be sufficient reduction for certain applications. However, solar light significantly improved the Fe^0/H$_2$O$_2$ treatment, resulting in 50% of COD removal, whereas up to 90% of COD removal was achieved in the presence of UV light.

95% of 1,4-dioxane was already degraded with the consumption of 20 kJ L^{-1}.

Due to the differences in lamp power and the range of the emitted light spectrum, solar photo-Fenton resulted in much lower reductions of organic matter (only slightly faster than the TiO$_2$-processes, Fig. 1). Namely, in Fe^0/H$_2$O$_2$/solar process about 65% of 1,4-dioxane was degraded with the consumption of approximately 480 kJ L^{-1}. Unlike in TiO$_2$-based photocatalysis, in the photo-Fenton processes the ratio of irradiated surface to reactor volume did not strongly affect the efficiency of 1,4-dioxane degradation. This is likely because the addition of Fe^0 microspheres did not cause such significant turbidity that would otherwise suppress light penetration. Therefore, the activation of Fe^0 occurred similarly in the bulk of the treated sample, and the process was only dependent on the nature and intensity of the light.

In contrast with TiO$_2$-photocatalysis (Fig. 3), only trace low concentrations of EGDF ($\leq$1.1 $\pm$ 0.1 mg L^{-1}) were detected throughout the Fe^0-based photo-Fenton processes, while significant concentrations of ethylene glycol were measured instead. Apparently, the type of radiation does not affect the degradation mechanism in heterogeneous photo-Fenton, since similar intermediates were detected with both UV and solar light. Namely, ethylene glycol and formic acid were found to be the major reaction intermediates, as shown for the Fe^0/H$_2$O$_2$/UV process in Fig. 4. In addition to formic acid, several other carboxylic acids were identified and monitored both by chromatographic analysis and FTIR spectrometry (Fig. 4A and B, respectively). Methoxyacetic and glycolic acids were generated starting at the beginning of the reaction, reaching maximum concentrations at 60 min and degrading slowly afterwards, while acetic and oxalic acids appeared later, accumulating to a lesser extent during the course of the reaction.
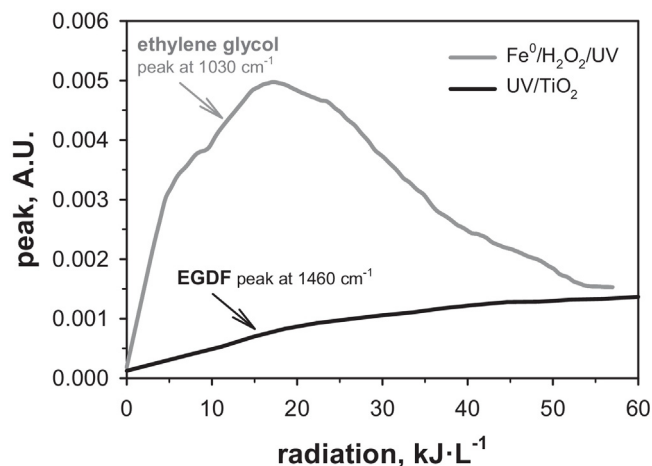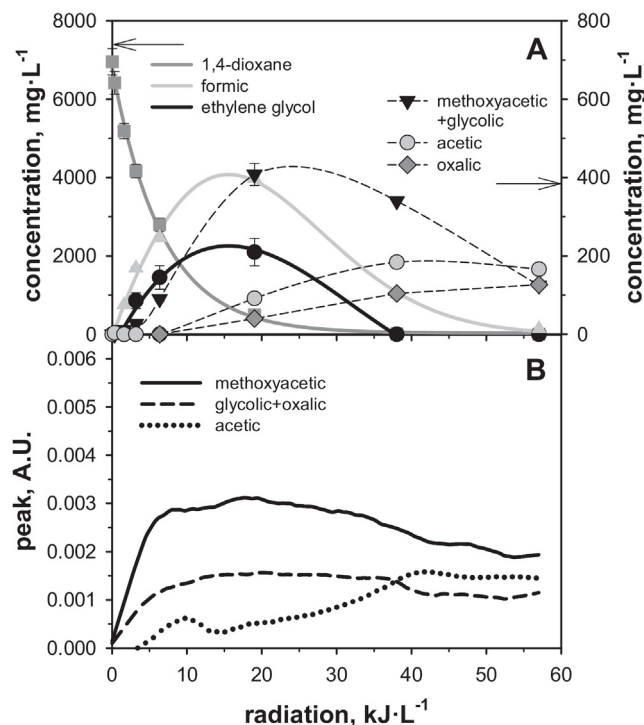

Fig. 4. Degradation products of 1,4-dioxane oxidation during heterogeneous Fe^0-based UV photo-Fenton process: (A) chromatographic analysis of the major reaction intermediates; (B) FTIR monitoring of the peaks of selected carboxylic acids in relative absorbance units (A.U.). $C_{0;dioxane}$ = 7050 mg L^{-1}; pH$_0$ 8.5.
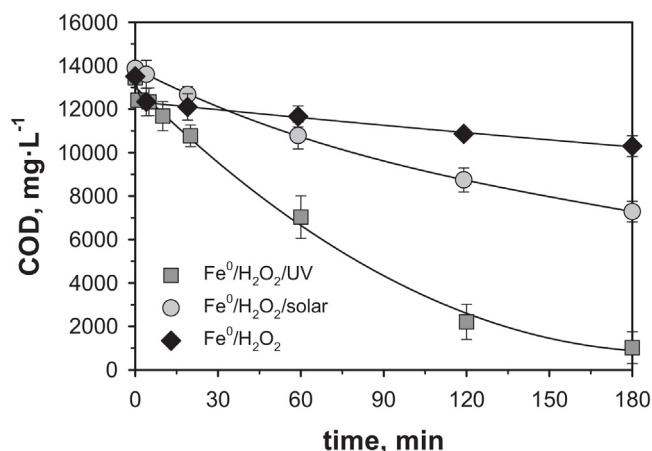
Fig. 5. Comparison of Fe^0-based heterogeneous photo-Fenton processes for 1,4-dioxane removal: (A) COD removal; (B) decrease of 1,4-dioxane peak in relative absorbance units (A.U.) monitored by FTIR spectrometry. $C_{0;dioxane} = 7050$ mg L^{-1}; pH_0 8.5.

Considering the degradation products of 1,4-dioxane and their subsequent decomposition, same compounds were detected in all three processes (Fe^0/H_2O_2, Fe^0/H_2O_2/solar and Fe^0/H_2O_2/UV), as described previously for the UV-catalyzed process (Fig. 4). However, reaction intermediates were measured in much lower quantities in Fe^0/H_2O_2 experiment (≤ 30 mg L^{-1}, data not shown). The earlier appearance and faster degradation of the reaction intermediates in UV-enhanced process is due to the greater activation of Fe^0 microspheres in the UV region than under solar radiation or in the absence of radiation. Thereby, greater activation of Fe^0 eventually results in greater hydroxyl radical ($^\bullet$OH) production and shorter reaction times.

3.2.2. Influence of iron source

For the sake of comparison, classical photo-Fenton with Fe^{2+} at highly acidic pH was also performed along with the heterogeneous photo-Fenton in basic conditions. With both iron sources ($FeSO_4$ and Fe^0), ethylene glycol and formic acid were the major reaction intermediates of 1,4-dioxane decomposition (Figs. 4 and 6, respectively). Although the same carboxylic acid by-products were detected using either $FeSO_4$ or Fe^0, much earlier and higher production of acetic acid was observed in heterogeneous photo-Fenton

with Fe^0. Apart from that, the main differences between classical and Fe^0-based photo-Fenton processes appear to lie in the reaction rate and the mineralization efficiency. Namely, the degradation of 1,4-dioxane was somewhat slower, the appearance of ethylene glycol later and the accumulation of formic acid greater with Fe^{2+}/H_2O_2/UV (Fig. 6) than with Fe^0/H_2O_2/UV (Fig. 4). In general, the final step of mineralization of the short chain carboxylic acids, e.g., oxalic acid, was slower with Fe^{2+} (75% of TOC removal) compared to the heterogeneous Fe^0-based treatment (85% of TOC removal).

The higher rates of 1,4-dioxane degradation and faster mineralization of the rest of the organics are most likely due to the Fe^{3+} recycle step in a so-called "pseudo-catalytic Fe^0/Fe^{2+} system", as reported previously by Bremner et al., Kallel et al. and Prousek et al. [41–44]. In agreement with other authors [30,34,45], Fe^0 is oxidized to Fe^{2+} in the presence of H_2O_2 and/or UV light, leading to the traditional Fenton reaction, producing ferric iron (Fe^{3+}). Fe^{3+} tends to form refractory ferric carboxylate complexes that, although eventually photo-decarboxylated by UV-light, can slow down the overall mineralization process [23,44,46]. Thus, Fe^0 microspheres present an advantage because, apart from the photo-recovery of catalytic Fe^{2+} similar to classical photo-Fenton, the Fe^{3+} produced during treatment also reacts with Fe^0, additionally regenerating Fe^{2+} to then proceed back to the Fenton reaction, producing more available $^\bullet$OH [41–44].

3.2.3. Influence of reagent dose

Fe^0-based photo-Fenton experiments using different patterns of H_2O_2 addition, demonstrated that the presence of excess H_2O_2 is crucial for the 1,4-dioxane oxidation on Fe^0 microspheres to take place at acceptable velocity. Namely, the best results were achieved with continuous H_2O_2 additions up to the stoichiometric ratio of $H_2O_2/COD_0 = 2.125$, whereby most of the 1,4-dioxane (>99%) was degraded with the consumption of less than 40 kJ L^{-1} and the subsequent degradation of the primary intermediate, ethylene glycol, was also almost completed. H_2O_2 was consumed slowly (about 53 mg L^{-1} per minute) while most of the oxidant was accumulated in solution during the experiment (Fig. 7A). Therefore, more than 15,000 mg L^{-1} of H_2O_2 was still present in the water at the end of the experiment, which would not be acceptable in industrial applications.

We studied whether a different pattern for the addition of H_2O_2 could reduce the amount of residual H_2O_2. Specifically, we added H_2O_2 only when the previous dosage was consumed, obtaining a rate of H_2O_2 disappearance of just 13 mg L^{-1} min^{-1} and only
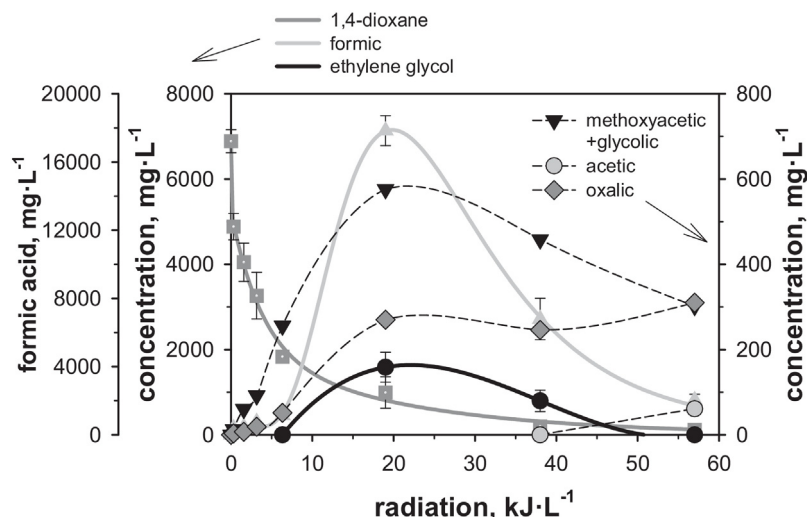

Fig. 6. Degradation products of 1,4-dioxane oxidation during homogeneous Fe^{2+}-based UV photo-Fenton process. $C_{0;dioxane} = 7050$ mg L^{-1}; pH_0 2.8.
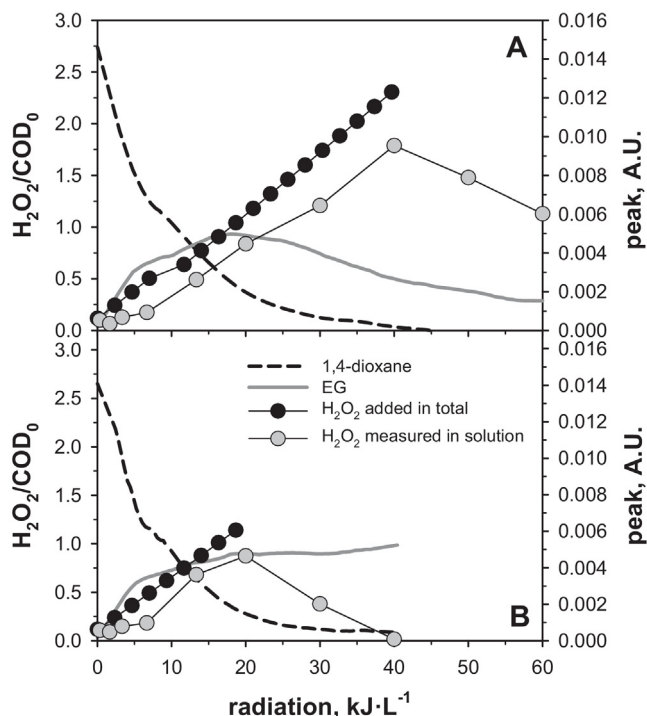
Fig. 7. FTIR monitoring of the peaks of 1,4-dioxane and ethylene glycol during heterogeneous Fe^0-based UV photo-Fenton processes (A) with continuous H_2O_2 additions up to the stoichiometric ratio of $H_2O_2/COD_0 = 2.125$; (B) with continuous H_2O_2 additions up to the ratio of $H_2O_2/COD_0 = 1.0625$ (50% of the stoichiometric ratio). $C_{0;dioxane} = 7050$ mg L^{-1}; pH_0 8.5.
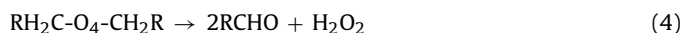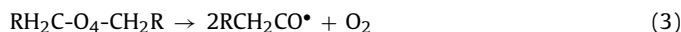
30% of 1,4-dioxane degradation with nearly 60 kJ L^{-1} of radiation. Therefore, it was concluded that at least an initial excess of H_2O_2 was needed for satisfactory removals. As a compromise, H_2O_2 was added continuously in short intervals only up to the ratio of $H_2O_2/COD_0 = 1.0625$ (50% of the stoichiometric ratio), as shown in Fig. 6B. However, oxidant addition was cut afterwards to estimate whether the excess of H_2O_2 accumulated in the system by that point was sufficient to proceed with the oxidation.

The on-line FTIR monitoring of both 1,4-dioxane and ethylene glycol indicated that the process with lower amount of H_2O_2 was less effective, as ethylene glycol began to accumulate when oxidant additions stopped (Fig. 7B). Nevertheless, nearly 97% of 1,4-dioxane, 65% of COD and 50% of TOC were removed along with the total consumption of the leftover H_2O_2. Moreover, the residual ethylene glycol is a biodegradable compound that should be easily removed in further treatment by conventional methods [47]. Therefore, nearly complete removal of 1,4-dioxane accompanied with the generation of biodegradable compounds could be reached by using only half of the stoichiometric amount of H_2O_2 required.

3.3. Comparison of degradation routes

Considering the above-presented results of light enhanced degradation of 1,4-dioxane with heterogeneous catalysts, the reaction pathways were proposed. The major routes of 1,4-dioxane degradation with the studied treatments are presented in a simplified schematic (Scheme 1). Most of the intermediate degradation steps omitted in Scheme 1 occur through radical intermediates following the mechanism of tetroxide formation over peroxyl radical, as described in detail by Cooper et al. and by von Sonntag and Schuchmann [48,49]. In principle, all the reactions with organics initiated by free radicals (e.g., •OH) lead to the formation of carbon-centered radicals [48]. These radicals (e.g., $RH_2C^{•}$) may react with dissolved O_2 to form peroxyl radicals (Eq. (1)), which normally

undergo bimolecular decay to form tetroxide intermediates (Eq. (2)) [48,49]. The production of two oxyl radicals and O_2 (Eq. (3)) and the generation of two carbonyl compounds and H_2O_2 (Eq. (4)) are two of the typical pathways suggested for the subsequent tetroxide decomposition [49,50].

$$RH_2C^{•} + O_2 \rightarrow RH_2CO_2^{•} \tag{1}$$

$$2RH_2CO_2^{•} \rightarrow RH_2C\text{-}O_4\text{-}CH_2R \tag{2}$$

$$RH_2C\text{-}O_4\text{-}CH_2R \rightarrow 2RCH_2CO^{•} + O_2 \tag{3}$$

$$RH_2C\text{-}O_4\text{-}CH_2R \rightarrow 2RCHO + H_2O_2 \tag{4}$$

As described by several authors, the source for the main primary intermediates of 1,4-dioxane is 1,4-dioxan-α-oxyl radical generated through the formation of tetroxide **I** (Scheme 1) [10,35,51], which is obtained in the reactions similar to Eqs. (1)–(3). In agreement with Stefan and Bolton [35], the α-oxyl radical was degraded either through ∆C–C splitting at the α-C position (route A, Scheme 1) or through an intramolecular reaction (H abstraction from the αí-C position) followed by fragmentation (route B, Scheme 1).

In route A (Scheme 1), another carbon-centered radical generated through an oxidative ring opening mechanism initiated by •OH is once again precursor for the formation of corresponding tetroxide (**II**) in reactions similar to Eqs. (1) and (2). **II** decomposes either to EGDF (Eq. (4)-type reaction) or alkoxyl radicals (Eq. (3)-type reaction) that lead to EGMF and formaldehyde [10,35,52]. Such decomposition of 1,4-dioxane through a linear tetroxide appears to be an important pathway for both heterogeneous AOPs, as EGDF and EGMF were detected in all the experiments, although the formation of EGDF seems to be predominant, as only trace concentrations of EGMF were detected.

The further decomposition of EGDF in UV/TiO$_2$ process is started with H-abstraction by •OH or HO$_2^{•}$ attack [35,51]. This O_2-demanding transformation process over another tetroxide intermediate may eventuate in either producing alkoxyl radicals (Eq. (3)-type) to give formic acid, glyoxal and glycolic acid as final products or generating ester intermediate (Eq. (4)-type) that hydrolyses to glycolic and formic acids [51,52].

The decay of EGDF in heterogeneous photo-Fenton oxidation, however, is different from photocatalytic degradation. Namely, in the pH conditions tested in the Fe^0-based photo-Fenton (pH_0 8.5; Fig. 4), EGDF is hydrolyzed rapidly into ethylene glycol (Scheme 2) [8]. Ethylene glycol was also reported as the primary intermediate in the classic Fenton process; however, in the latter, ethylene glycol was generated through an acidic hydrolysis of EGDF (pH_0 2.8)
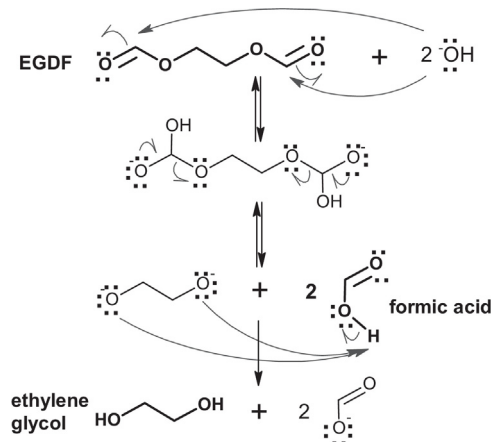
Scheme 2. Decomposition route for the basic hydrolysis of EGDF into ethylene glycol.
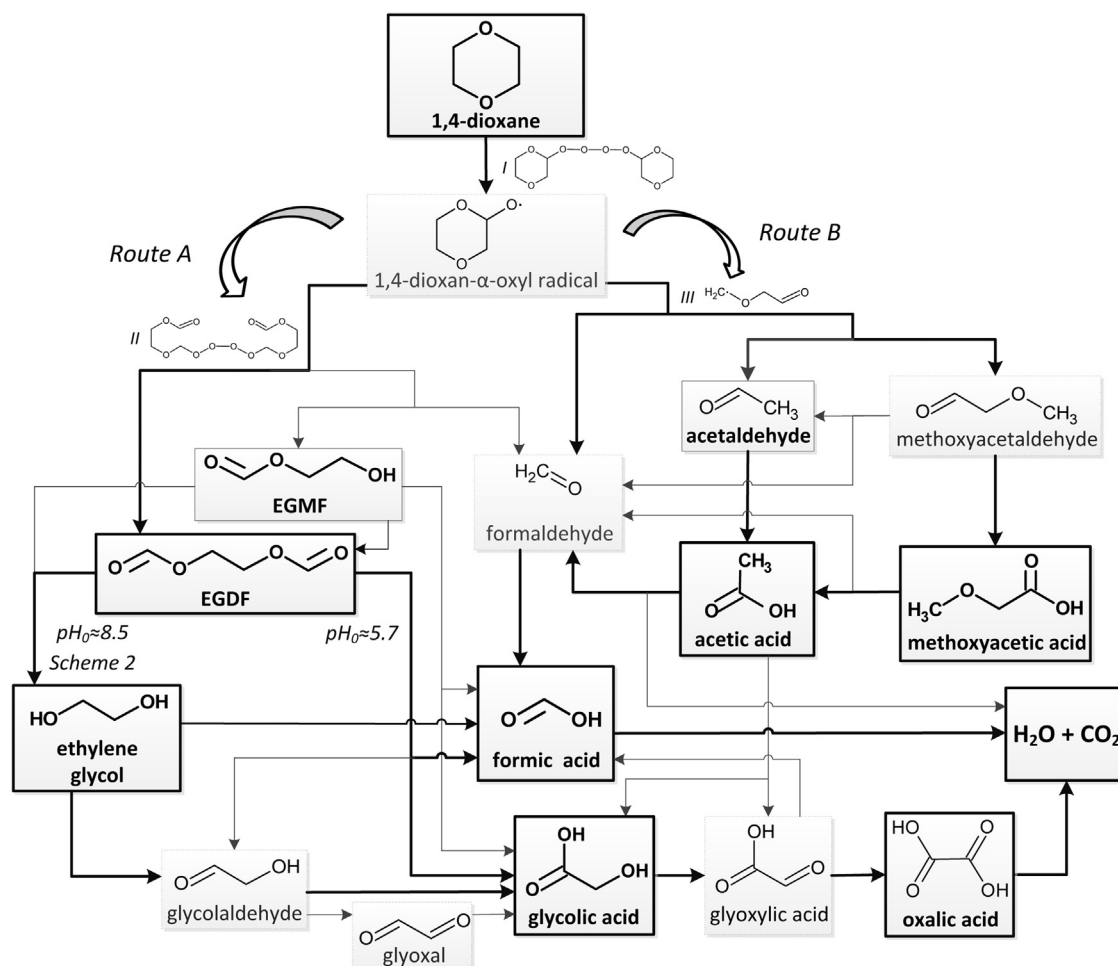
Scheme 1. Simplified schematic of 1,4-dioxane decomposition routes.

[10]. Therefore, similar a pathway of acid-catalyzed hydrolysis is expected to occur in the $Fe^{2+}/H_2O_2/UV$ process (Fig. 6). Regardless of the cause of hydrolysis, ethylene glycol is subsequently degraded to glycolic acid through the formation of glycolaldehyde [10,53], whereas possible generation of some formic acid has been reported as well [53,54].

The major difference between the two heterogeneous AOPs is due to the variation in pH profile because the operating pH of UV/TiO_2 process (pH_0 5.7) was neither acidic nor basic enough for the hydrolysis of EGDF to ethylene glycol to occur. Nevertheless, both AOPs continued through the decomposition of carboxylic acids towards final mineralization. In further oxidation, formic acid is directly mineralized to CO_2 [35,48] at a high reaction rate with $\cdot OH$ (Table 1) [55]. Glycolic acid decomposes to glyoxylic acid which is next rapidly oxidized to oxalic acid [10,48,56]. Oxalic acid appears as one of the most common last detected intermediates before the mineralization of organics [8,35,48]. To a lesser extent, some glyoxylic acid could also decompose to formic acid, which is easily degraded to water and CO_2 [48,56].

According to the general tendency, the rate constants of acids for reactions with $OH\cdot$ are smaller than those of their anions (Table 1) [55–57]. This could probably be the reason for the faster TOC removal and lesser accumulation of carboxylic acids in $Fe^0/H_2O_2/UV$ process at pH_0 8.5 than in $Fe^{2+}/H_2O_2/UV$ oxidation at pH_0 2.8 because at neutral and slightly basic conditions most of the carboxylic acids under question are in their dissociated form. The accumulation of carboxylic acids could also negatively affect the initial decomposition of 1,4-dioxane, as they compete with the parent compound for the oxidants [35].

Another major difference between the Fe^0-catalyzed and Fe^{2+}-based photo-Fenton processes is apparently the greater importance of an alternative degradation route B (Scheme 1) in $Fe^0/H_2O_2/UV$ process. Namely, in the alternative route B, according to Stefan and Bolton [35], 1,4-dioxan-α-oxyl radical is degraded through an intramolecular reaction producing formaldehyde and, thus,

Table 1
Physicochemical constants of the studied carboxylic acids.

Acid/anion	pK_a	Aqueous phase reaction rate constant with $OH\cdot$ ($M^{-1} s^{-1}$)
Acetic acid		$1.6 \times 10^{7\,a}$
Acetate ion	4.75	$8.5 \times 10^{7\,a}$
Formic acid		$1.4 \times 10^{8\,a}$
Formate ion	3.75	$3.2 \times 10^{9\,a}$
Glycolic acid		$6.0 \times 10^{8\,a}$
Glycolate ion	3.83	$8.6 \times 10^{8\,a}$
Glyoxylic acid		$3.6 \times 10^{8\,b}$
Glyoxylate ion	3.20	$2.6 \times 10^{9\,b}$
Methoxyacetic acid		NF
Methoxyacetate ion	3.57	NF
Oxalic acid		$1.4 \times 10^{6\,a}$
Hydrogen oxalate ion	1.27/4.27	$4.7 \times 10^{7\,a}/1.9 \times 10^{8\,b}$
Oxalate ion		$7.7 \times 10^{6\,a}/1.6 \times 10^{8\,b}$

NF: Not found.
[a] Buxton, 1988.
[b] Ervens, 2003.

formic acid along with the carbon-centered radical (**III**) (Scheme 1). **III** is either reduced to methoxyacetaldehyde which is subsequently oxidized to methoxyacetic and acetic acids or undergoes β-scission yielding acetaldehyde and, consequently, acetic acid [10,35,36]. Comparing the profiles of acetic acid during the two photo-Fenton processes (Figs. 4 and 6), it seems to be the presence of Fe^0 that brings about the considerable production of acetic acid (Fig. 4), indicating the more pronounced occurrence of degradation route B (Scheme 1). The subsequent degradation of acetic acid gives formaldehyde, and glycolic and glyoxylic acids as major by-products in free-radical-induced degradation, whereas CO_2 is produced as well, indicating that some mineralization also occurs in that stage of decomposition [48,56,58].

On the other hand, relatively low concentrations of acetic acid were detected only at the very end of the Fe^{2+}-based photo-Fenton experiment (Fig. 6). Therefore, the mixed profile of methoxyacetic and glycolic acids in the $Fe^{2+}/H_2O_2/UV$ oxidation (Fig. 6) at greater extent probably belongs to glycolic acid produced in the degradation of ethylene glycol (route A, Scheme 1). With regard to UV/TiO_2 oxidation, considering the profiles of both methoxyacetic and acetic acids, the alternative route B was hardly significant in TiO_2-photocatalytic process (Fig. 2).

4. Conclusions

FTIR was successfully applied as a powerful tool for the mechanistic study and optimization of the heterogeneous AOPs. On-line FTIR study supported by an extensive chromatography analysis allowed the establishment of the major decomposition pathways of 1,4-dioxane. EGDF was detected as the major primary intermediate in TiO_2-photocatalysis, whereas ethylene glycol was found as the main initial by-product in Fe^0 based photo-Fenton, generated through the basic hydrolysis of EGDF due to the different pH profile. An alternative route of 1,4-dioxane degradation into methoxyacetic and acetic acids was also observed, being more pronounced in photo-Fenton processes and accentuated in the presence of Fe^0. Regardless, the decomposition of primary intermediates in both AOPs continued over the generation of short chain carboxylic acids, formic acid being the most prevalent intermediate by-product.

Heterogeneous $Fe^0/H_2O_2/UV$ oxidation yielded complete removal of 1,4-dioxane and 85% mineralization of TOC, outperforming the classical photo-Fenton process (75% of TOC), most likely owing to the improved regeneration of Fe^{2+} from Fe^{3+}. Solar light could work as cost-effective alternative for the activation of Fe^0 microspheres, achieving 65% removal of 1,4-dioxane. Although constant addition of H_2O_2 in excess was crucial for the rapid oxidation on Fe^0, the FTIR monitoring showed that significant degradation along with the production of biodegradable by-products is reached by using only half of the stoichiometric amount of H_2O_2 required to degrade the organic matter.

Almost 60% of 1,4-dioxane was degraded in TiO_2-photocatalysis; however, longer radiation times should lead to higher degradation (considering the almost linear removal with both UV and solar light (≈ 7.5 mg kJ^{-1})). Unlike in heterogeneous photo-Fenton processes where the Fe^0 microspheres did not produce any significant turbidity, the ratio of irradiated surface to reactor volume greatly affected the heterogeneous photocatalysis where activation of TiO_2 particles was expected to occur mainly on the irradiated liquid surface.

Acknowledgements

References

[1] T.K.G. Mohr, Environmental Investigation and Remediation: 1,4-Dioxane and Other Solvent Stabilizers, CRC Press, Boca Raton, 2010.
[2] European Chemicals Bureau (ECB), E.U. Risk Assessment Report: 1,4-Dioxane (ISBN 92-894-1252-6), Second Priority List 21, 1–129; Office for Official Publications of the European Communities, Luxembourg, 2002.
[3] U.S. Environmental Protection Agency (USEPA), Toxicological Review of 1,4-Dioxane (CAS No. 123-91-1), EPA/635/R-09/005-F, USEPA, Washington, DC, 2010.
[4] National Industrial Chemical Notification and Assessment Scheme (NICNAS), Full Public Report: 1,4-Dioxane. Priority Existing Chemical No. 7, Australian Government Publishing Service, Canberra, 1998.
[5] U.S Environmental Protection Agency (USEPA), Treatment Technologies for 1,4-Dioxane: Fundamentals and Field Applications, EPA-542-R-06-009, USEPA, Office of Solid Waste and Emergency Response, Washington, DC, 2006.
[6] J.M. Skadsen, B.L. Rice, D.J. Meyering, A Case Study in the City of Ann Arbor, Water Utilities, City of Anna Arbor, and Fleis & VendenBrink Engineering Inc., 2004.
[7] M.J. Zenker, R.C. Borden, M.A. Barlaz, Environ. Eng. Sci. 20 (2003) 423–432.
[8] H. Barndõk, L. Cortijo, D. Hermosilla, C. Negro, A. Blanco, J. Hazard. Mater. 280 (2014) 340–347.
[9] H. Barndõk, D. Hermosilla, L. Cortijo, E. Torres, A. Blanco, Environ. Sci. Pollut. Res. 21 (2014) 5701–5712.
[10] N. Merayo, D. Hermosilla, L. Cortijo, Á. Blanco, J. Hazard. Mater. 268 (2014) 102–109.
[11] M.H. So, J.S. Han, T.H. Han, J.W. Seo, C.G. Kim, Water Sci. Technol. 59 (2009) 1003–1009.
[12] J.H. Suh, M. Mohseni, Water Res. 38 (2004) 2596–2604.
[13] A. Fujishima, T.N. Rao, D.A. Tryk, J. Photochem. Photobiol. C 1 (2000) 1–21.
[14] A.L. Linsebigler, G.Q. Lu, J.T. Yates, Chem. Rev. 95 (1995) 735–758.
[15] D. Hermosilla, N. Merayo, R. Ordonez, A. Blanco, Waste Manage. 32 (2012) 1236–1243.
[16] C.P. Huang, C. Dong, Z. Tang, Waste Manage. 13 (1993) 361–377.
[17] E. De Torres-Socias, I. Fernandez-Calderero, I. Oller, M.J. Trinidad-Lozano, F.J. Yuste, S. Malato, Chem. Eng. J. 234 (2013) 232–239.
[18] C. Mendoza-Marin, P. Osorio, N. Benitez, J. Hazard. Mater. 177 (2010) 851–855.
[19] I. Oller, S. Malato, J.A. Sanchez-Perez, M.I. Maldonado, W. Gernjak, L.A. Perez-Estrada, J.A. Munoz, C. Ramos, C. Pulgarin, Ind. Eng. Chem. Res. 46 (2007) 7467–7475.
[20] T.F.C.V. Silva, A. Fonseca, I. Saraiva, V.J.P. Vilar, R.A.R. Boaventura, Water Res. 47 (2013) 3543–3557.
[21] P.A. Soares, T.F.C.V. Silva, D.R. Manenti, S.M.A.G.U. Souza, R.A.R. Boaventura, V.J.P. Vilar, Environ. Sci. Pollut. Res. 21 (2014) 932–945.
[22] B.S. Souza, F.C. Moreira, M.W.C. Dezotti, V.J.P. Vilar, R.A.R. Boaventura, Catal. Today 209 (2013) 201–208.
[23] D. Hermosilla, M. Cortijo, C.P. Huang, Chem. Eng. J. 155 (2009) 637–646.
[24] H.M. Coleman, V. Vimonses, G. Leslie, R. Amal, Water Sci. Technol. 55 (2007) 301–306.
[25] T. Vescovi, H.M. Coleman, R. Amal, J. Hazard. Mater. 182 (2010) 75–79.
[26] C.N. Chang, Y.S. Ma, G.C. Fang, A.C. Chao, M.C. Tsai, H.F. Sung, Chemosphere 56 (2004) 1011–1017.
[27] N. Merayo, D. Hermosilla, L. Blanco, L. Cortijo, A. Blanco, J. Hazard. Mater. 262 (2013) 420–427.
[28] D. Hermosilla, M. Cortijo, C.P. Huang, Sci. Total Environ. 407 (2009) 3473–3481.
[29] R.F.F. Pontes, J.E.F. Moraes, A. Machulek, J.M. Pinto Jr., J. Hazard. Mater. 176 (2010) 402–413.
[30] J.J. Pignatello, E. Oliveros, A. MacKay, Crit. Rev. Environ. Sci. Technol. 36 (2006) 1–84.
[31] H. Barndõk, L. Blanco, D. Hermosilla, Á. Blanco, Chem. Eng. J 284 (2016) (2016) 112–121.
[32] V. Maurino, P. Calza, C. Minero, E. Pelizzetti, M. Vincenti, Chemosphere 35 (1997) 2675–2688.
[33] E. Khan, W. Wirojanagud, N. Sermsai, J. Hazard. Mater. 161 (2009) 1024–1034.
[34] H.-S. Son, J.-K. Im, K.-D. Zoh, Water Res. 43 (2009) 1457–1463.
[35] M.I. Stefan, J.R. Bolton, Environ. Sci. Technol. 32 (1998) 1588–1595.
[36] H.-S. Kim, B.-H. Kwon, S.-J. Yoa, I.-K. Kim, J. Chem. Eng. Jpn. 41 (2008) 829–835.
[37] APHA, AWWA, WPCF (Eds.), Standard Methods for the Examination of Water and Wastewater, Washington, DC, 2005.
[38] H. Pobiner, Anal. Chem. 33 (1961) 1423–1428.
[39] N. Merayo, D. Hermosilla, C. Negro, A. Blanco, Chem. Eng. J. 232 (2013) 519–526.
[40] X. Liang, X. Zhu, E.C. Butler, J. Hazard. Mater. 190 (2011) 168–176.
[41] D.H. Bremner, A.E. Burgess, D. Houllemare, K.C. Namkung, Appl. Catal. B: Environ. 63 (2006) 15–19.

[42] M. Kallel, C. Belaid, R. Boussahel, M. Ksibi, A. Montiel, B. Elleuch, J. Hazard. Mater. 163 (2009) 550–554.

[43] M. Kallel, C. Belaid, T. Mechichi, M. Ksibi, B. Elleuch, Chem. Eng. J. 150 (2009) 391–395.

[44] J. Prousek, E. Palackova, S.A. Priesolova, L. Markova, A. Alevova, Sep. Sci. Technol. 42 (2007) 1505–1520.

[45] J.A. Bergendahl, T.P. Thies, Water Res. 38 (2004) 327–334.

[46] V. Kavitha, K. Palanivelu, Chemosphere 55 (2004) 1235–1243.

[47] W.K. Shieh, J.A. Lepore, I. Zandi, Water Sci. Technol. 38 (1998) 145–153.

[48] W.J. Cooper, C.J. Cramer, N.H. Martin, S.P. Mezyk, K.E. O'Shea, C. von Sonntag, Chem. Rev. 109 (2009) 1302–1345.

[49] C. von Sonntag, H.-P. Schuchmann, Peroxyl radicals in aqueous solutions, in: Z. Alfassi (Ed.), Peroxyl Radicals, John Wiley, New York, 1997, pp. 173–234.

[50] J.E. Bennett, R. Summers, Can. J. Chem. Rev. Can. Chim. 52 (1974) 1377–1379.

[51] M.A. Beckett, I. Hua, Environ. Sci. Technol. 34 (2000) 3944–3953.

[52] H. Barndõk, D. Hermosilla, C. Han, D.D. Dionysiou, C. Negro, Á. Blanco, Appl. Catal. B: Environ. 180 (2016) 44–52.

[53] The Dow Chemical Company, http://dowac.custhelp.com/app/answers/detail/a_id/11979, 2014, (accessed 13.03.2015).

[54] W.J. Rossiter, P.W. Brown, M. Godette, Sol. Energy Mater. 9 (1983) 267–279.

[55] G.V. Buxton, C.L. Greenstock, W.P. Helman, A.B. Ross, J. Phys. Chem. Ref. Data 17 (1988) 513–886.

[56] N. Karpel Vel Leitner, M. Dore, Water Res. 31 (1997) 1383–1397.

[57] B. Ervens, S. Gligorovski, H. Herrmann, Phys. Chem. Chem. Phys. 5 (2003) 1811–1824.

[58] Y. Tan, Y.B. Lim, K.E. Altieri, S.P. Seitzinger, B.J. Turpin, Atmos. Chem. Phys. 12 (2012) 801–813.